SCIENCE CHINA
Chemistry

• REVIEWS •

HOT PAPER

June 2016 Vol.59 No.6: 659–671

• SPECIAL TOPIC •Molecular Functional Materials and Applications

doi: 10.1007/s11426-015-5520-9

Flexible and stretchable electrodes for next generation polymer electronics: a review

Dustin Chen, Jiajie Liang & Qibing Pei*

Department of Materials Science and Engineering, University of California, Los Angeles, School of Engineering and Applied Science and California Nanosystems Institute, CA 90095, USA

Received September 18, 2015; accepted October 6, 2015; published online January 7, 2016

Transparent conductive electrodes play a significant role in the fabrication and development of optoelectronic devices. As next generation optoelectronic devices tend towards mobile and wearable devices, the added attribute of flexibility or stretchability for these electrodes becomes increasingly important. However, mechanical requirements aside, transparent conductive electrodes must still retain high transparency and conductivity, with the metrics for these parameters being compared to the standard, indium tin oxide. In the search to replace indium tin oxide, two materials that have risen to the forefront are carbon nanotubes and silver nanowires due to their high transparency, conductivity, mechanical compliance, and ease of fabrication. This review highlights recent innovations made by our group in electrodes utilizing carbon nanotubes and silver nanowires, in addition to the use of these electrodes in discrete devices and integrated systems.

transparent conductive electrode, carbon nanotube, silver nanowire, flexible, stretchable, OLED

Citation: Chen D, Liang JJ, Pei QB. Flexible and stretchable electrodes for next generation polymer electronics: a review. *Sci China Chem*, 2016, 59: 659−671, doi: 10.1007/s11426-015-5520-9

1 Introduction

In recent years, wearable electronics have transformed from a concept once posited by writers of science fiction to a functional reality permeating the everyday lives of everyday people. With the rapid development of these next generation electronics, the search for high performing flexible or stretchable transparent conductive electrodes (TCEs) has been highlighted as a critical barrier to surmount before the realization of high efficiency, high performance optoelectronic devices. In the selection of TCEs, the two parameters most commonly discussed are high conductivity and transparency [1], with these parameters being compared to the standard, indium tin oxide (ITO). Adding to these two parameters, next generation TCEs must also exhibit mechanical compliancy, retaining their properties under various applied loadings and strains.

Carbon based materials such as carbon nanotubes [2,3] (CNTs) and graphene [4,5] have been identified as a potential candidate due to desirable mechanical properties, in addition to having electrical and optical properties that allow for the fabrication of certain electrical devices. Furthermore, these carbon electrodes can be solution processed [1,6], allowing for high speed, low cost, row-to-roll processing, in contrast with traditional ITO electrodes requiring expensive batch-based processing.

Networks of metallic nanowires have also been shown to exhibit high transparency, conductivity, and mechanical compliancy, and like carbon-based materials, can be solution processed. In particular, silver nanowires (AgNW) have garnered significant attention, being used for applications

*Corresponding author (email: qpei@seas.ucla.edu)

ranging from organic light emitting diodes (OLEDs) [7–9], solar cells [8,10,11], transparent heaters [12], thin film transistors [13,14], to electronic circuits [15]. These AgNW based devices have exhibited comparable performance, or in some cases, exceeded the performance of devices fabricated using traditional electrode technology.

The aforementioned TCEs are by no means an exhaustive list of alternative TCE technology. As an example, graphene has similarly garnered significant interest in electrode technology. Due to its high Fermi-velocity and the ability to be doped, graphene films exhibit extremely high in-plane conductivities [1]. Wu *et al.* [16] demonstrated OLEDs on graphene substrates approaching the performance of ITO based devices. Furthermore, due to the mechanical properties of this carbon based material, graphene based electrodes can be fabricated to be flexible or stretchable [4], and can similarly be roll-to-roll processed [5]. However, though pristine graphene is an excellent candidate for a TCE, the difficulties in fabricating high quality films render the material cumbersome to use. Due to their combination of optoelectric and mechanical performance, and their time and fiscal efficient fabrication, carbon nanotubes and silver nanowires are currently at the forefront to replace ITO in next generation optoelectronics. The present review first highlights the fabrication, development, and advancements we have made in recent years in the field of CNT and AgNW based electrodes. Second, we elucidate upon the use of these electrodes to fabricate discrete devices and integrated systems. Finally, we conclude with an outlook and future research challenges.

2 Flexible electrodes

2.1 Carbon nanotube flexible electrodes

For the simplest flexible electrodes, a conductive medium can be deposited on top of a flexible substrate. These easily fabricated electrodes possess high transparency and conductivity, as the use of nanotubes leads to a percolation network, with the relatively large amounts of open areas between adjunct nanotubes leading to high transparency. The conductivity is dictated by the intrinsic conductivity of the material, in addition to the junction-junction resistance between individual carbon nanotubes.

Yu *et al.* [17,18] fabricated carbon nanotube based flexible electrodes by depositing a solution of raw carbon nanotubes on a polyethylene terephthalate (PET) substrate. To obtain a uniform dispersion of CNTs, raw CNTs were admixed with sodium dodecylsulfonate, a surfactant, in a water solution before high-power ultrasonication [18]. The dispersion was filtered onto a film and rinsed with deionized water to remove extra surfactant, before being transferred to a PET substrate using a polydimethylsiloxane (PDMS) stamp [18].

Resulting flexible electrodes yielded sheet resistances of 500 ohm/□ at a transparency in the visible spectrum of 85% [18]. The bonding between the CNT network and the PET was sufficiently strong to not delaminate through ultrasonic cleaning and immersion in various solvents [18]. Most importantly, the SWNT electrodes exhibited attractive mechanical properties, as bending the electrode to a 12.5 mm radius resulted in a negligible change in the sheet resistance of the electrode [17].

Limitations of the flexible carbon nanotube electrode described above include an excessively high sheet resistance for certain applications, and various other physical properties that may limit the efficacy of the TCE. The high surface roughness arising from the finite thickness of the stacked nanotubes on PET are detrimental to the performance of organic or polymer light emitting diodes (OLEDs, PLEDs), which may manifest in large shorts and reduced efficiency. Furthermore, the large energy offset between the Fermi level of the CNTs and the lowest unoccupied molecular orbital (LUMO) of typical conjugated polymers prohibit efficient transfer of charges, resulting in low-performance devices. These inherent limitations are addressed with the development of flexible silver nanowire electrodes.

2.2 Silver nanowire flexible electrodes

In a typical fabrication, AgNW flexible electrodes are fabricated by first coating a layer of AgNWs from a dispersion of isopropyl alcohol (IPA) and methanol through wet deposition techniques such as drop casting, Meyer rod coating, dip coating, or spin coating onto a smooth release substrate. A bifunctional monomer with photoinitiator is overcoated on top of the AgNW coating, infiltrating the pores between the nanowires, and contacting the underlying release substrate [19–21]. After UV irradiation to crosslink the monomer, the flexible freestanding film is peeled off, resulting in an embedded AgNW network inlaid within a polymer matrix. The flexible electrode exhibits good mechanical properties, being shown to withstand bending at a 4 mm radius for 1000 cycles without deterioration of electrical properties [22].

The AgNW films can be tailored to the desired transparency and conductivity by controlling the amount of solid nanowires deposited on the release surface, as shown in Figure 1(a) [21]. At transparency of 82%, freestanding films have a sheet resistance of approximately 10 ohm/□, comparable to commercially available ITO on PET substrates, and significantly higher than the typical 200 ohm/□ value observed for flexible CNT electrodes [21].

In addition, embedding the AgNW within a polymer matrix drastically decreases the surface roughness, making devices such as OLEDs or solar cells built on top of the electrode significantly more efficient in contrast to rough electrodes with the same sheet resistance. Figure 1(b) illustrates the AFM topographical image of an embedded AgNW electrode at a sheet resistance of 10 ohm/□ [19]. The average surface roughness for these embedded elec-

trodes can be up to one order of magnitude lower than those described in the previous section detailing CNT electrodes. The use of AgNWs instead of CNTs also lowers the barrier for charge injection into conjugated polymers, further increasing efficiency for optoelectronic devices built on top.

Additional degrees of variability can be introduced into the electrode by selection of the polymer matrix. Li *et al.* [22] embedded the AgNW percolation network within a heat resistant acrylate material to allow for subsequent device fabrication requiring temperatures up to 200 °C. Yu *et al.* [21] used a shape memory acrylate to reform and refreeze the electrode into new shapes when heated and cooled above the glass transition temperature (T_g) of the polymer. The electrodes can further be made to be stretchable with the introduction of stretchable polymer matrices.

3 Stretchable electrodes

3.1 Carbon nanotube stretchable electrodes

Similar to CNT based flexible electrodes, the simplest CNT stretchable electrodes consist of CNTs deposited on the surface of a stretchable medium, as seen in the SEM image in Figure 2(a) [23]. In several previous studies, single walled CNTs (SWCNTs) were spray coated on a dielectric elastomer, partially embedding the SWCNTs within the surface of the polymer [23–25]. The electrodes were reported to be capable of resisting uniaxial strains in excess of 150%, or cycled at strains of 120% for thousands of cycles without an appreciable increase in sheet resistance [24]. The resistance change as a function of cycles is shown in Figure 2(b) [24]. Furthermore, minimal changes in mechanical properties after cycling were observed across a broad temperature range [24].

To make the CNT stretchable electrode more applicable for applications requiring smooth surfaces, Yu *et al.* [26] embedded SWCNT networks within a stretchable poly(tert-butyl acrylate) (PtBA) matrix to obtain freestanding electrodes with 77% transparency at a sheet resistance of 200 ohm/□. It was observed that the conductivity of the SWCNT networks increased up to a strain of 35% due to an alignment of nanotubes along the stretching direction, which facilitates charge transport within the electrode [26]. Similar to nanotubes deposited on top of a stretchable substrate, the embedded nanowires showed stable performance

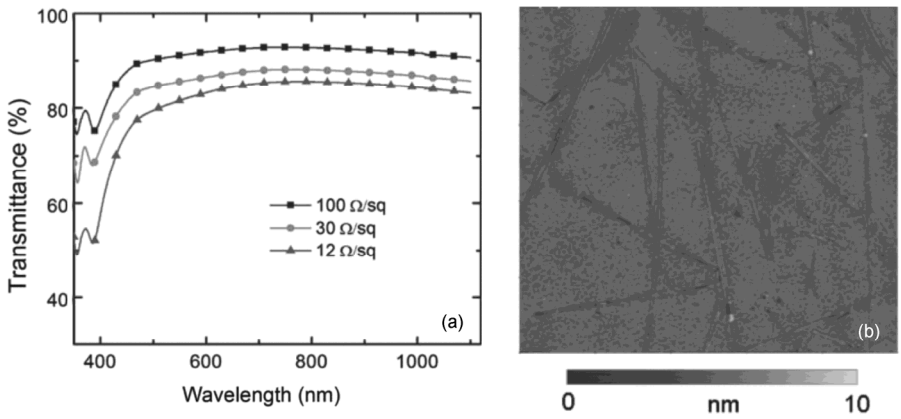

Figure 1 (a) Transmittance as a function of wavelength for AgNW-acrylate freestanding electrodes at different sheet resistances. (b) AFM topographical image of a freestanding AgNW-acrylate embedded electrode with a sheet resistance of 10 ohm/□. Reprinted with permission from refs. [21,19]. Copyright {2011} Wiley-VCH.

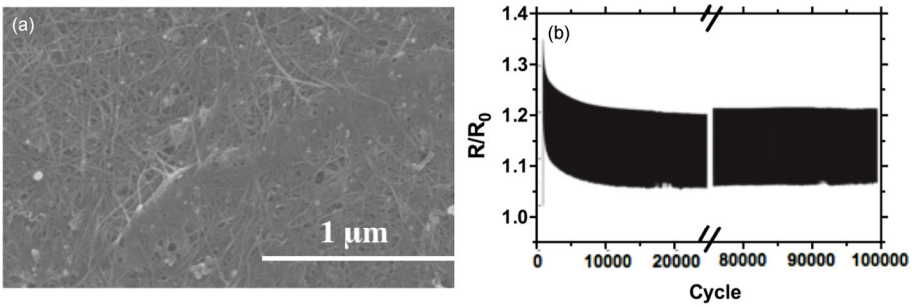

Figure 2 (a) SEM image of SWCNT spray coated on a VHB 4910 acrylic adhesive film from 3M. (b) Cycle lifetime test for a SWCNT electrode stretched to 100% strain at a strain rate of 1000% per second. Reprinted with permission from ref. [23], Copyright {2008} Wiley-VCH and ref. [24], Copyright {2014} Wiley-VCH, respectively.

after extended cycling tests.

These two types of stretchable CNT electrodes served as the basis for the further development of stretchable electrodes. Though the optoelectric performance of these electrodes may be sufficient for certain applications, higher conductivity and transparency are required for others. Furthermore, due to the relatively weak bonding force between the CNT and polymer matrix, incomplete transfer from the release substrate to the polymer may result in a rough surface, further limiting the applicability of these electrodes for applications requiring a high degree of smoothness.

3.2 Silver nanowire stretchable electrodes

As a significant amount of optoelectronic applications requiring high conductivity and transparency similarly require low surface roughness, all silver nanowire based stretchable electrodes were fabricated by embedding the nanowires within a polymer matrix [27–31]. In the fabrication of stretchable electrodes, the selection of the polymer matrix is paramount to the performance, with selection criteria involving parameters including the bonding between nanowires and polymer, glass transition temperature, modulus, and transparency.

Yun *et al.* [28] embedded the AgNWs in a copolymer of *tert*-butly acrylate (TBA) and acrylic acid (AA) to form a stretchable electrode with shape memory properties. Though TBA by itself exhibits good elasticity and shape memory performance, the hydrophobicity of the homopolymer results in poor bonding with the nanowires. The addition of AA allows increased bonding between the copolymer and AgNWs via the carboxylic acid group, preventing sliding between the nanowires and polymer during repeated stretching cycles, and thus, minimizing the rate of increase of resistance when stretched. However, excessive concentrations of AA raises the T_g value of the copolymer, leading to prohibitively high power consumptions for the electrode if used for shape memory applications. Figure 3 illustrates the evolution of the nanowire electrodes with increasing strain, and cyclical testing, with various weight percentages of AA added [28]. A weight percentage of 5% AA was seen to improve the overall stretchability of the electrode both in uniaxial stretching and in cyclical testing. These electrodes were found to recover 98% of the resistance change after relaxing the electrode following stretching at 30% strain, 95% at 70% strain, and 90% at 90% strain, verifying the efficacy of the TCE as a stretchable electrode [28]. Lower recovery at higher strains were correlated with the viscoelasticity of the polymer matrix, exhibiting irreversable damage at high strains.

For stretchable electrodes not requiring shape memory properties, Hu *et al.* [29] embedded the AgNW within an elastomeric polyurethane (PU) matrix. The freestanding electrodes exhibited a sheet resistance of 8 ohm/□ at a transparency of 75%, similar to the transparency value observed on the release glass substrate [29]. Using the rubbery PU matrix, the stretchable electrode was able to be reversibly stretched up to 170% strain, with the strained electrodes rapidly relaxing back to its original shape upon removal of the external load.

The AgNWs themselves can be manipulated as well to obtain enhanced performance. Liang *et al.* [31] soldered the nanowires with a thin layer of graphene oxide (GO) before embedding the nanowires within the polymer matrix. Fabrication of the GO-soldered AgNWs remained largely the same as the general process for stretchable AgNW electrode fabrication, with the introduction of a soaking step in a 1 mg/mL GO dispersion in distilled water and IPA following AgNW coating on a release substrate. The SEM image in Figure 4(a) shows that the percolation network remains intact, though a GO layer is evident at the nanowire junctions. This fusing at the nanowire junction is able to prevent inter-nanowire sliding at the junctions when the composite electrode is stretched. Figure 4(b) shows the stretching performance of the composite electrode after the GO-soldered AgNWs are embedded within a polyurethane matrix, with a non-GO soldered AgNW stretchable electrode for comparison. The GO-soldered AgNWs were seen to have smaller

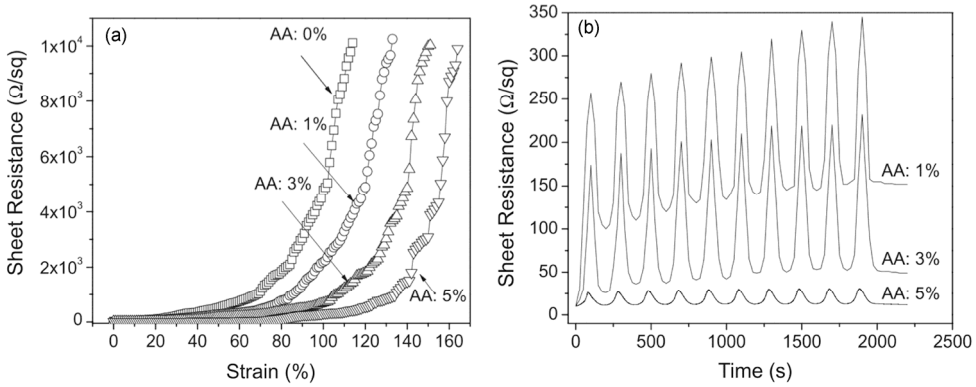

Figure 3 (a) Change in sheet resistance of stretchable AgNW-TBA/AA composite electrode with increasing strain. (b) Change in sheet resistance of stretchable AgNW composite during 10 cyclic loadings of strain between 0 and 50% strain at a constant strain rate of 0.005 /s. Reprinted with permission from ref. [28]. Copyright {2014} Wiley-VCH.

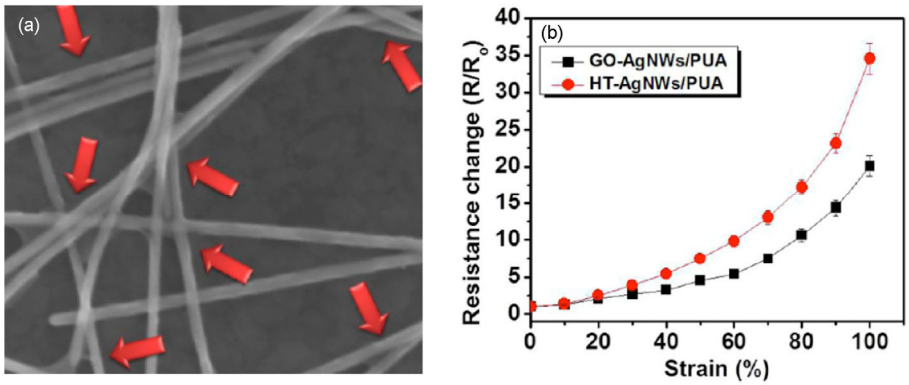

Figure 4 (a) GO-soldered AgNW networks, with fused junctions indiciated by red arrows. (b) Normalized resistance of GO-AgNW-PU and AgNW-PU electrodes stretched at 1 mm/s (20%/s) (color online). Reprinted with permission from ref. [31]. Copyright {2014} American Chemical Society.

resistance increase with strain in contrast to the control device, increasing in resistance by 2.3, 5.3, and 10.6-fold at strains of 40%, 60%, and 80%, respectively. In contrast, the control electrode increased 5.4, 9.8, and 17.2 fold.

These electrodes described above are the basis of several optoelectronic devices. Detailed description of these devices will be elucidated upon in further sections.

4 Flexible lighting

4.1 Flexible light emitting electrochemical cell

In previous work, rigid light emitting electrochemical cells have been fabricated on ITO [32,33]. Briefly, the polymer LEC consists of a single active layer consisting of a light emitting polymer (LEP), an electrolyte to supply dopants, and an ionic conductor sandwiched between two electrodes. The LEC exhibits light emitting properties due to the formation of a dynamic p-i-n junction in the polymer layer upon application of a bias, which effectively removes the charge injection barrier at the polymer-electrode interfaces [33]. The formation of excitons from the recombination of electrons and holes near this junction is the mechanism of light formation for these devices. Though the performance of polymer LECs (PLECs) lag behind polymer LEDs, the use of a single polymer layer that can be wet processed is highly appealing, resulting in thorough investigation through the years in increasing the stability, luminance, and efficiency of these devices.

However, the use of ITO as the anode still requires one component requiring expensive batch based vacuum processing, in addition to rendering the LEC rigid, as the electrode material is well known to be brittle even under low loadings. Yu *et al.* [17] fabricated a PLEC using spray coated SWCNT on PET as both the anode and cathode. Though conventional light emitting devices require high smoothness for optimal performance, the high thicknesses of the emissive layer that can be utilized within PLECs without sacrificing performance render this method of electrode fabrication sufficient. PF-B, a blue emissive luminescent polymer, an ethoxylated trimethylopropane triacrylate (ETT-15) as the ionic conductor, and lithium trifluoromethan sulfonate (LiTf) as the salt were used as the polymer layer in a weight ratio of 20:10:1, respectively [17]. The polymer was spin-coated onto the SWCNT/PET anode, with the resulting stack subsequently laminated underneath another SWCNT/PET cathode using a roll lamination machine at 120 °C [17]. For flat devices, the PLEC had a turn-on voltage of 3.8 V, a maximum intensity of 1400 cd/m^2 at 10 V, and a maximum efficiency of 2.2 cd/A at 480 cd/m^2 [17]. The device performance (current density and luminance as a function of voltage, and efficiency as a function of luminance) is shown below in Figure 5. No change in light emission intensity and uniformity was observed after being bent to a 2.5 mm radius. Furthermore, as seen in Figure 5(a), the electrical characteristics of the blue-emission devices remained virtually identical after being bent to a 2.5 mm radius, highlighting the efficacy of the two SWCNT based flexible electrodes. A slight decrease in efficiency was observed in the bent device, as seen in Figure 5(b).

Liang *et al.* [34] demonstrated a PLEC using a bilayer SWCNT/AgNW anode fabricated by sequentially Meyer rod coating layers of SWCNTs and AgNWs before embedding the hybrid conductive percolation layer in a urethane acrylate, difunctional methacrylate monomer, and tert-butyl acrylate monomer mixture. The use of the bilayer anode is to improve the area coverage of conductive material; AgNWs by themselves yield relatively low surface coverage, resulting in non-uniform charge injection, and non-active regions of emission. Yellow PLECs were fabricated with the bilayer electrode as anode, an active layer comprising SuperYellow as the emissive material, a cross-linked trimethylolpropanetriacrylate (ETPTA) as an ionic conductor, LiTf as the salt, and an evaporated aluminum (Al) layer as cathode [34]. To evaluate the performance of the bilayer anode, the same devices were also fabricated on control anodes of ITO/glass and a single AgNW layer composite

electrode.

The performance of the yellow PLECs on the three anodes described above are shown in Figure 6. Figure 6(a) illustrates the *J-V* curve of the devices. The bilayer composite electrode has higher current density than both devices on ITO/glass and the AgNW composite electrode. This high current density is a result of the low resistivity of the highly conductive AgNW network, in conjunction with the uniform surface coverage due to the small dimensions of the SWCNT network. The high current density leads to high charge injection, and thus, high emission intensity. Because the area coverage of the bilayer electrode is higher than that of the AgNW electrode, there is more charge distribution into the emissive layer, leading to a larger lighted area. Thus, the emission characteristics of the bilayer anode device are higher than that of the AgNW electrode, and resemble those devices built on ITO/glass, as seen in Figure 6(b). Furthermore, the efficiency of the PLEC on the composite electrode exceeds that on ITO/glass (Figure 6(c)). This can be attributed in part by the surface plasmon scattering of emitted light by the nanowires, increasing the out-coupling efficiency [34].

The PLECs described demonstrate the viability of various flexible electrodes for use in flexible lighting devices. For high performance light emitting devices, similar technology can be employed with organic LEDs (OLEDs).

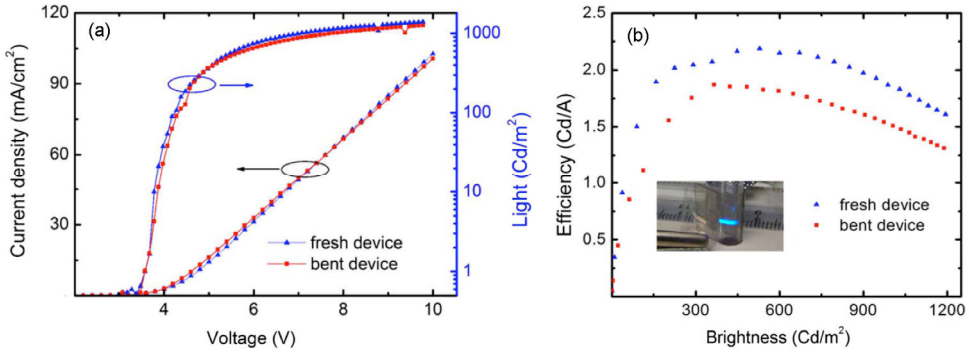

Figure 5 (a) Current and light emission as a function of voltage for a bent and flat blue-emission device. (b) Efficiency as a function of brightness of a bent and flat blue-emission device, with bent device shown in inset (color online). Reprinted with permission from ref. [17]. Copyright {2009} American Institute of Physics.

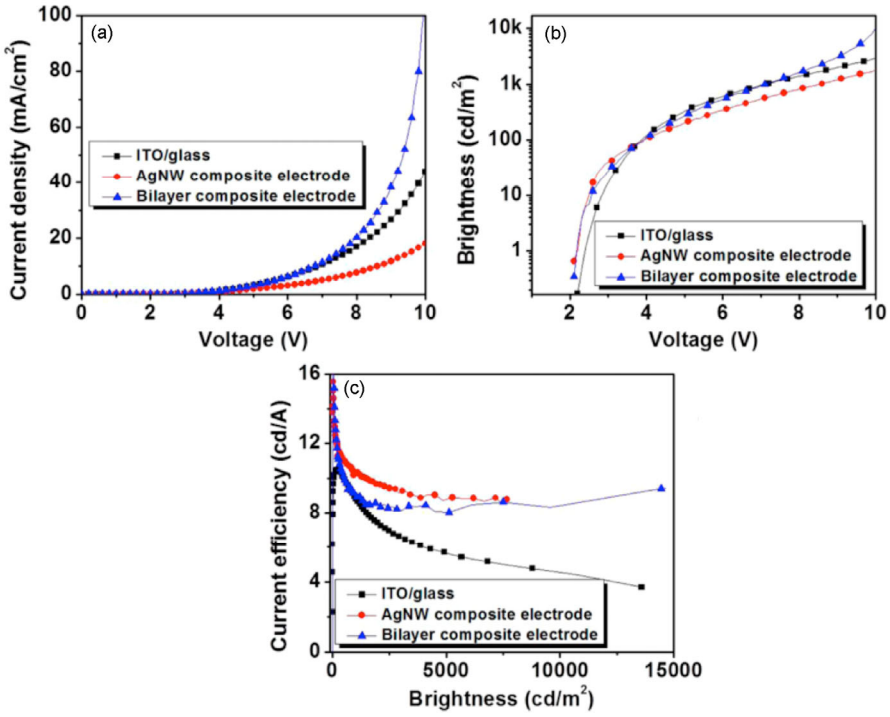

Figure 6 (a) *J-V* characterisitics of yellow PLEC fabricated on a bilayer anode, a mono-layer AgNW anode, and ITO/glass. (b) Luminance-voltage characteristics of a yellow PLEC fabricated on the three different anodes. (c) Current efficiency as a function of brightness for yellow PLECs fabricated on the three different anodes (color online). Reprinted with permission from ref. [34]. Copyright {2013} American Chemical Society.

4.2 Flexible organic light emitting diodes

Though OLEDs or PLEDs require additional processing in contrast with PLECs, the enhancement in performance, stability, and efficiency largely outweigh the additional time and fiscal costs brought about by the more complex fabrication. Like the aforementioned PLECs, AgNW or hybrid AgNW/SWCNT substrates provide a cost and performance efficient platform to build OLEDs or PLEDs on top of them. Several devices for a variety of different applications have been reported using these composite electrodes as the basis [20,21,35,36]. Yu *et al*. [21] fabricated shape-memory PLEDs using a bifunctional acrylate polymer as the matrix supporting the AgNWs for the anode, followed by subsequent layers of poly(3,4-ethylenedioxythiophene) polystyrene sulfonate (PEDOT:PSS) as a hole injection layer (HIL), an alkoxyphenyl substituted yellow emissive poly-(1,4-phenylene vinylene) (SY-PPV), cesium fluoride (CsF) as the electron injection layer (EIL), and Al as the cathode. To evaluate the shape change properties and performance of the PLED, the device was heated above the T_g of the polymer substrate, bent to a 2.5 mm radius, and relaxed back to the flat shape. The devices were able to operate at a high brightness during the shape change process occurring at 120 °C, as seen in Figure 7(a) [21]. Furthermore, the current efficiency of the device remains unchanged at approximately 14 cd/A after several cycles of bending and recovery, as seen in Figure 7(b) [21]. The operational lifetime of the PLED was also similar to control devices fabricated on ITO, with the emission intensity reducing to 80% of its maximum value after 24 hours of continuous operation, in contrast to the 88% observed with ITO as the anode. This difference in lifetime may be due to a higher operating voltage needed to drive the AgNW based devices.

For higher efficiency lighting, Li *et al.* [35] fabricated white polymer phosphorescent LEDs (WPLED) using the AgNW composite substrates. Like the previously discussed PLED, the WPLED fabricated was fully solution processed for low fabrication cost, using PEDOT:PSS as the HIL and CsF and Al as the EIL and cathode, respectively. The emissive layer comprised a mixture of host material poly(vinylcarbazole) (PVK) and electron transporting (ET) material 1,3-bis[4-*tert*-butylphenyl)-1,3,4-oxidiazolyl] phenylene (OXD-7), doped with blue phosphorescent dopant bis[4,6-difulorophenyl)-pyridinato-N,C^2] (picolinato) Ir(III) (FIrpic), green phosphorescent dopant tris(2-(4-toyl) pyridinato-N,C^2) (Ir((mppy)$_3$), and red phorphorescent dopant bis(1-phenylisoquinoline) (acetylacetonate) (IR(piq)). PVK was selected as the host due to its high triplet energy level, good surface topography, thermal stability, and its ability to conduct holes.

It was reported that the use of the AgNW polymer substrate had the additional benefit of extracting more light emitted from the emissive layer in comparison to devices built on ITO/glass. Figure 8 illustrates the architecture of the WPLEDs on both ITO/glass and AgNW/polymer. Due to total internal reflection, light beams emitted at small angles (L1 and L2) from the WPLED on ITO/glass are trapped. However, the composite substrate has a twofold benefit. First, the AgNWs serve to scatter light, allowing smaller angle rays (R1) to change course, and be extracted from the opposite side of the substrate. Second, the index mismatch between emissive layer and polymer substrate is smaller than that between emissive layer and ITO, allowing wider angles to be extracted from the WPLED.

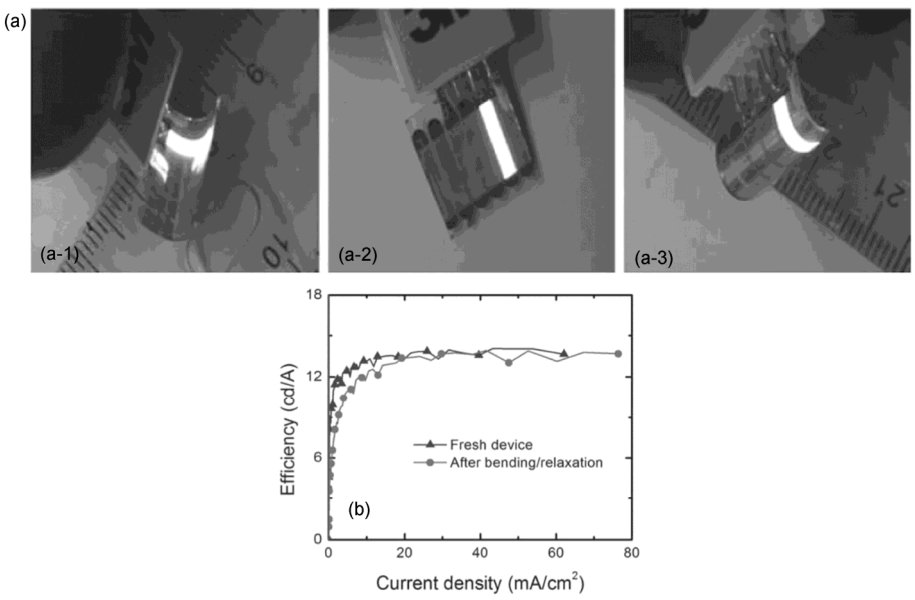

Figure 7 (a) Shape memory PLEDs bent and frozen to a 2.5 mm radius (a-1), recovered to flat position (a-2), and bent and frozen to the opposite direction (a-3). (b) Current efficiency as a function of current density for fresh PLEDs, and PLEDs subjected to 10 cycles of bending and recovery. Reprinted with permission from ref. [21]. Copyright {2011} Wiley-VCH.

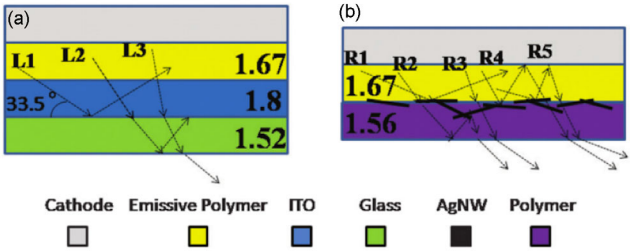

Figure 8 Schematic cross-sectional views of WPLEDs on ITO/glass (left), and AgNW/polymer (right). The refractive index of the layers are shown in the schematic, in addition to the modes of light extraction in the devices (color online). Reprinted with permission from ref. [35]. Copyright {2011} Royal Society of Chemistry.

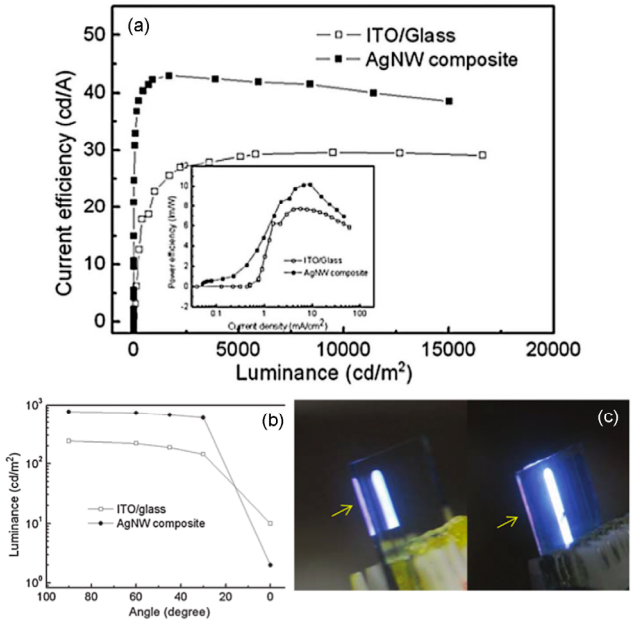

Figure 9 (a) Current efficiency as a function of luminance for WPLEDs fabricated on ITO/glass and AgNW/polymer power efficiency as a function of current density is shown in the inset. (b) Luminance as a function of angle. (c) Electroluminance photograph of WPLEDs on ITO/glass (left) and AgNW/polymer (right) during operation, with arrows pointing to the location of edge emission (color online). Reprinted with permission from ref. [35]. Copyright {2011} Royal Society of Chemistry.

As a result of the enhanced light extraction of WPLEDs built on AgNW/polymer, the current efficiency measured exceeded that of control devices fabricated on ITO/glass by 41% [35]. Current density as a function of luminance and power density as a function of current density are shown in Figure 9(a). A maximum current efficiency of 42.3 cd/A for the three primary color device, with the current density remaining in a narrow range around 40 cd/A up to a luminance of 10,000 cd/m^2, as seen in Figure 9(a) was obtained. The enhanced light extraction is quantified in Figure 9(b), where a higher luminance is observed at all angles except extremely low angles in the AgNW/polymer WPLED in contrast to WPLEDs fabricated on ITO/glass. This can empirically be observed in Figure 9(c), with both a wider viewing angle for the AgNW/polymer WPLED, and a significantly weaker edge emission due to a majority of the light being extracted from the substrate.

To further increase the efficiency of WPLEDs, Li *et al.* [36] dispersed nanoparticles of barium strontium titante (BST) in a AgNW/SWCNT/polymer matrix. Using finite-difference time-domain (FDTD) analysis, the light extraction enhancement as a function of diameter and refractive index of the nanoparticle (Figure 10(a)) was determined. A maximum enhancement of 3.61 was obtainable for nanoparticle diameters of 500 nm and a refractive of 2.6, when the doping concentration was 1 wt%. The peak enhancement factor as a function of wt% was also simulated (Figure

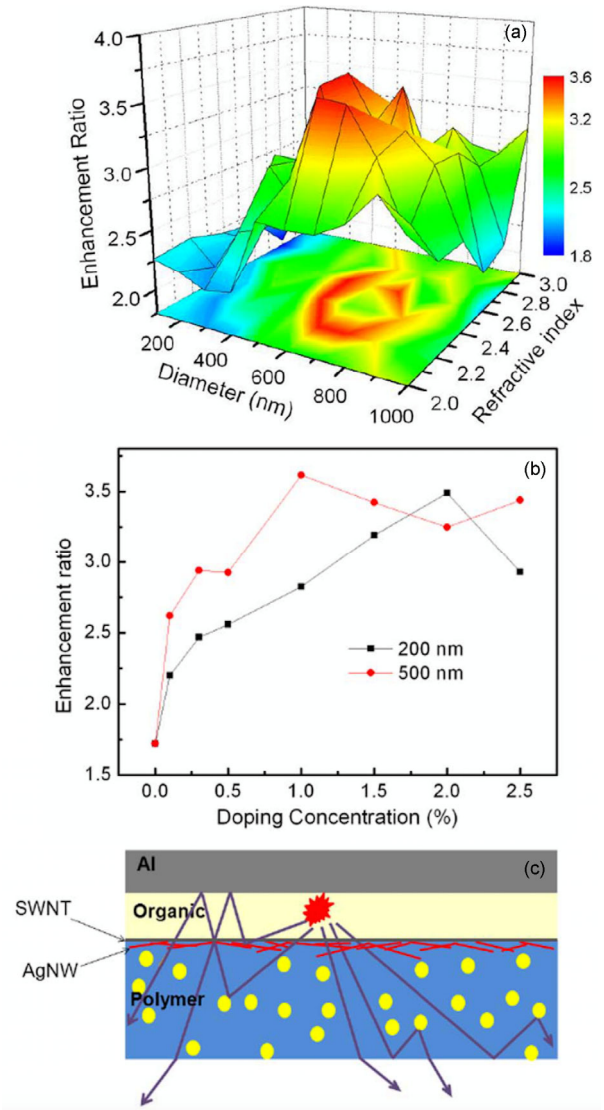

Figure 10 (a) Simulated enhancement in WPLEDs as a function of diameter and refractive index of nanoparticles dispersed within the substrate. (b) Simulated enhancement factors as a function of doping concentrations with the refractive index fixed at 2.6. (c) Schematic cross section of the AgNW/polymer substrate with nanoparticles dispersed illustrating the light scattering by the nanoparticles (color online). Reprinted with permission from ref. [36]. Copyright {2014} Nature Publishing Group.

10(b)), with 1 wt% being the optimal concentration for 500 nm BST nanoparticles, and 2 wt% being optimal for 200 nm nanoparticles. Figure 10(c) illustrates the benefit of using BST dispersed within the polymer matrix. With the nanocomposite polymer matrix, two major trapping modes in PLEDs fabricated on ITO/glass are eliminated or suppressed: (1) the waveguide mode in ITO is eliminated; and (2) the glass mode is suppressed as light propagation can be altered by the nanoparticles and nanowires.

Following simulation results, SWCNT/AgNW/polymer electrodes were fabricated with 2 wt% of 200 nm BST nanoparticles dispersed within the polymer matrix [36]. The 200 nm nanoparticles were selected instead of larger dimension nanoparticles due to the ease of dispersion of smaller nanoparticles within the acrylate monomer. WPLEDs were fabricated with a sandwich structure of Al/CsF/emissive layer/PEDOT:PSS/anode, with the emissive layer being a blend of a white polymer (WP) and OXD-7 in a 100:40 wt. ratio. As control devices, WPLEDs were fabricated on an additional four substrates: ITO/glass; AgNW/polymer; SWCNT/AGNW/polymer; and AgNW/BST/polymer. Figure 11 shows the current and power efficiency of the AgNW/SWCNT/BST/polymer, compared to the four reference devices. The values of current, power, and external quantum efficiency of the AgNW/SWCNT/BST/polymer based device were 44.7, 44.0, and 28.8, respectively, representing an enhancement of 119%, 140%, and 120% compared to respective values obtained from devices built on ITO/glass. The efficacy of the BST nanoparticles in enhancing the efficiency was seen in the enhancement of current, power and external quantum efficiencies of 55%, 48%, and 82% compared to SWCNT/AgNW/polymer based devices [36].

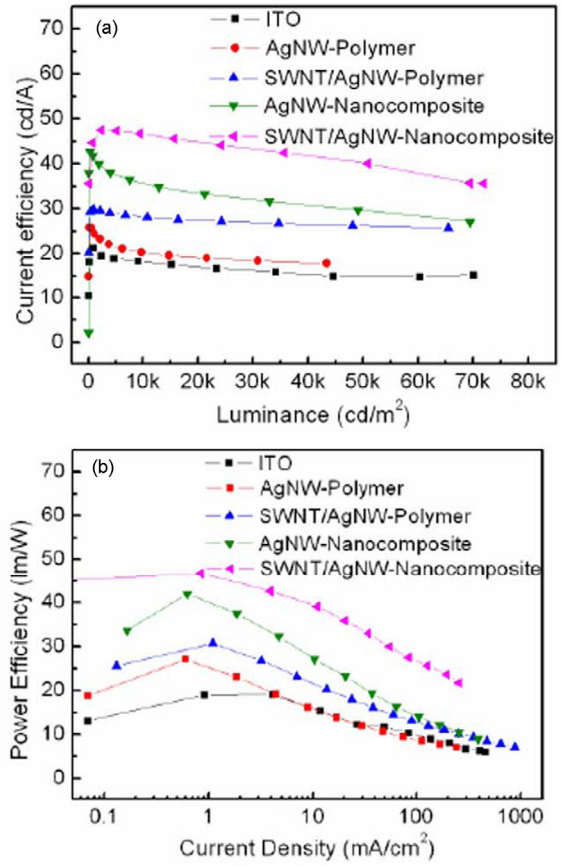

Figure 11 (a) Current efficiency as a function of luminance for WPLEDs fabricated on five different substrates. (b) Power efficiency as a function of current density for WPLEDs fabricated on five different substrates (color online). Reprinted with permission from ref. [36]. Copyright {2014} Nature Publishing Group.

The OLEDs described in this section verify the efficacy of AgNW or AgNW/SWCNT based electrodes for different applications. Careful selection and engineering of the polymer matrix can be used to tailor the properties desired for specific W/PLEDs. The same type of engineering can be applied to various stretchable electronics.

5 Stretchable electronics

5.1 Stretchable lighting

Yu *et al.* [26] first fabricated stretchable PLECs on SWCNTs embedded in a shape memory PtBA matrix. The PLECs consisted of the stretchable SWCNT electrodes sandwiching an emissive layer comprising a blue emissive polyfluorene copolymer (Pf-B); poly(ethylene oxide) dimethacrylate ether (PEO-DMA), an ionic conductor, and LiTf as the salt. To analyze the compliance of the PLECs, the devices were heated above the T_g of the shape memory polymer, anchored on two edges of a home-made stretching apparatus, and prestrained by 10% to flatten the device. The PLECs were subsequently stretched an additional 20% and 45%, and cooled to room temperature to freeze the deformed shape.

Emissions from the stretched devices were observed to be uniform throughout the active layer. Though the current density and luminance decrease with increasing strain, the efficiency exhibits slight enhancement at larger strains, as seen in Table 1.

For improved PLEC performance, Liang *et al.* [30] used embedded AgNWs in a rubbery poly(urethane acrylate) (PUA) matrix. The PLEC was fully solution processed with an emissive layer comprising SuperYellow as a yellow light emitting polymer, ETPTA as the ionic conductor, PEO as a

Table 1 Electroluminescence characteristics of the stretchable PLEC driven at 8 V at different strains. Reprinted with permission from ref. [26]. Copyright {2011} Wiley-VCH.

Property	Longitudinal strain		
	0%	20%	45%
Luminance (cd/m)	45	30	18
Current density (A/m^2)	59.4	35.7	20.8
Efficiency (cd/A)	0.76	0.84	0.87

second ionic conductor to enhance the stretchability of the ETPTA network, and LiTf as the salt, sandwiched between two AgNW-PUA electrodes. To avoid damage to the electrode from solvent attack, a thin layer of PEDOT:PSS was spun on the anode side prior to the deposition of the emissive layer.

The PLEC turned on at 6.8 V, and reached a peak brightness of 2200 cd/m^2 [30]. Unstretched, an EQE of 4.0% was obtained, comparable to state of the art PLECs based on SuperYellow on ITO at the time. When stretched, these devices increased in brightness up to 20% strain, then decreased at higher strains up to 120%, at which point light emission was no longer observed. Because the opposite trend was observed in current density, the current efficiency initially increases up to 80% strain, before leveling off and decreasing gradually until 120% strain. The current density exhibited this opposite trend due to an increase in sheet resistance of the composite electrode.

Due to the mechanical robustness of the device, the PLEC can be stretched, bended, or collapsed, promising easily deployable lighting that can conformally attach on non-uniform surfaces. Figure 12 illustrates the device stretched to various strains, and wrapped around the edge of a 400 micron thick piece of cardboard. The high flexibility and stretchability of the composite electrode allow the device to operate under these extreme conditions while maintaining uniform and bright emission.

Liang *et al*. [31] also fabricated stretchable white PLEDs using a graphene oxide soldered AgNW electrode embedded in a PUA matrix. The devices were fabricated with the architecture: GO-AgNW/PUA anode; PEDOT:PSS as the hole transport layer (HTL); an emissive layer comprising a white light emitting polymer and OXD-7; and a second GO-AgNW/PUA electrode coated with polythylenimine (PEI) acting as an electron transport layer (ETL). The performances of these devices were comparable to that observed with the stretchable PLEC. These stretchable lighting devices pave the foundation for rollable displays and other consumer tunable electronics of the future.

5.2 Stretchable transistor and display

For display technology, thin film transistor (TFT) arrays are required to control the pixels. In the case of stretchable lighting, a stretchable TFT array is a critical component in the development of a fully functioning stretchable display. Liang *et al.* [37] demonstrated an intrinsically stretchable, fully solution processed TFT using an AgNW/PUA elec-

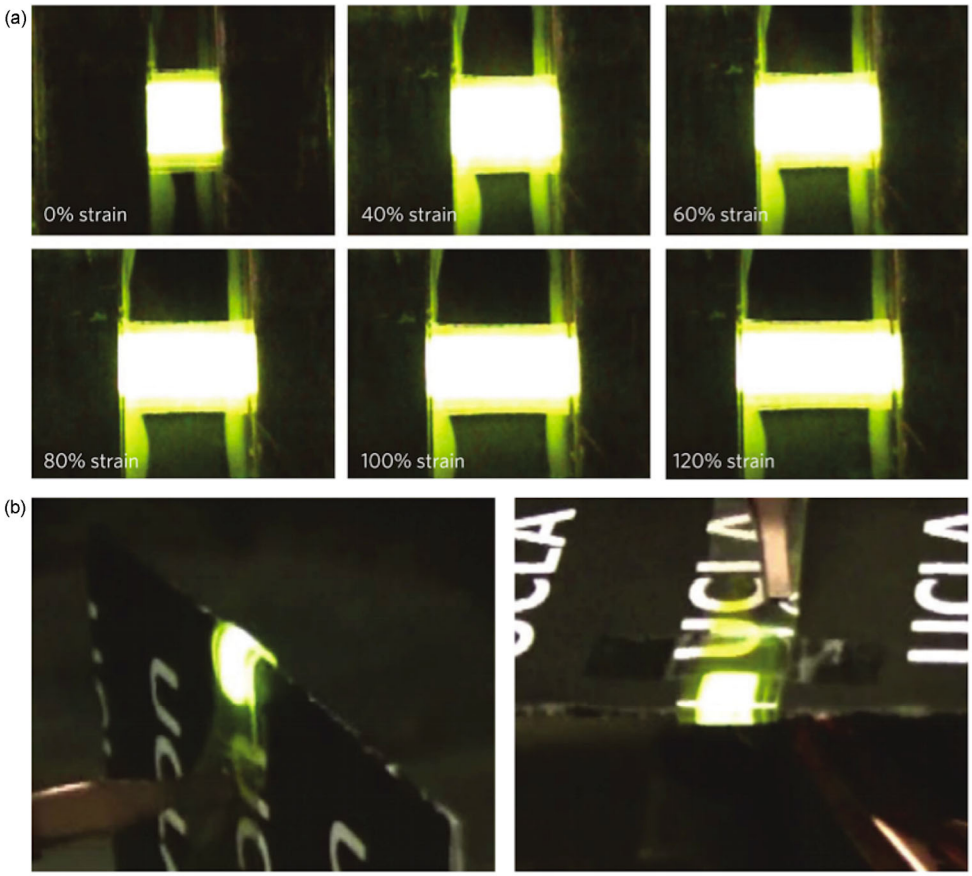

Figure 12 (a) PLECs stretched from 0–120% strain. (b) PLECs bent around a 400 micron thick piece of cardboard (color online). Reprinted with permission from ref. [30]. Copyright {2013} Nature Publishing Group.

trode as the source and drain, SWCNT as the network channel, and polyacrylate-*co*-polyethylene glycol (PA-*co*-PEG) as an elastomeric dielectric.

Transfer characteristics and device performance under applied strain are shown in Figure 13. A mobility of 30 $cm^2/(V\ s)$ was obtained, with an on-off ratio of 10^3–10^4, switching current>100 μA, and transconductance>50 μS [37]. At a strain of 50%, the mobility decreased to 16.2, due to the decrease in capacitance from the dielectric layer, while the on-off ratio remains relatively constant from strains ranging from 0–50%. In addition, the TFT was able to undergo repeated stretching of 20% strain over hundreds of cycles without significant loss in electrical property.

As a proof of concept of the efficacy of the stretchable TFT, the device was connected to a white-light OLED with the structure architecture glass/ITO/PEDOT:PSS/white emissive polymer layer/CsF/Al [37]. The *I*-*V* characteristics of the OLED connected circuit are shown in Figure 14(a), showing the device lighting up slowly as the voltage is increased. Good diode behavior with clear cutoff and triode region is observed in Figure 14(b), indicating the ability of the TFT to control the OLED.

The OLED test circuit was further characterized when the TFT was stretched under 0, 20%, and 30% strain. At higher strains, the field-effect behavior characteristic of TFTs is still observed (Figure 15(a)), verifying the efficacy of the TFT to operate under strains to drive lighting devices. Though I_{ON} decreases slightly with elevated strains, the current is still high enough to drive the lighting device. This decrease in current at higher strains is manifested in a decrease in brightness (68% decrease when stretched up to 30%). However, even with reduced luminance, the brightness is still sufficient for display applications. The luminance of the OLED under different inputs is shown in Figure 15(b).

Although the TFT was not used to drive a stretchable PLED, the demonstrated proof of concept highlights the potential efficacy of this technology in stretchable display technology with the further improvement of materials, fabrication procedure, and processing. These integrated systems give hope to the future of widely available, efficient stretchable devices for a vast array of applications.

6 Conclusions and outlooks

Carbon nanotubes and silver nanowires have been shown to display outstanding properties such as high transparency, conductivity, and mechanical compliance. Due to their ability to form a percolation network, these conductive materi-

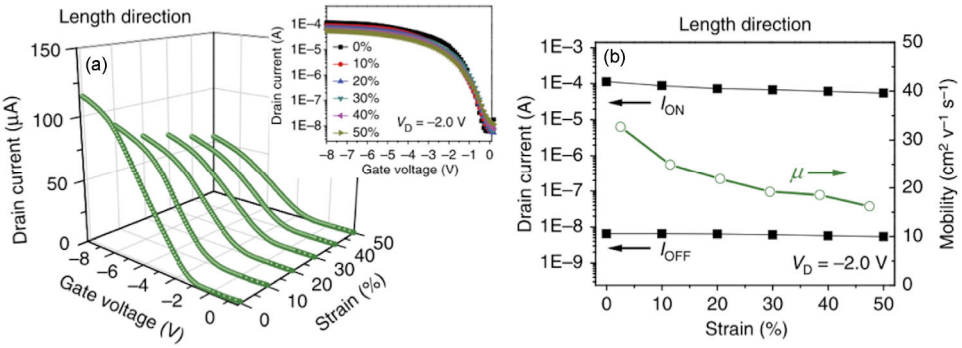

Figure 13 (a) Transfer characteristics ($V_{D=}$–2.0 V) of the stretchable TFT under strain. (b) $I_{ON,}$ I_{OFF}, and mobility as a function of applied strain along the channel length direction (color online). Reprinted with permission from ref. [37]. Copyright {2015} Nature Publishing Group.

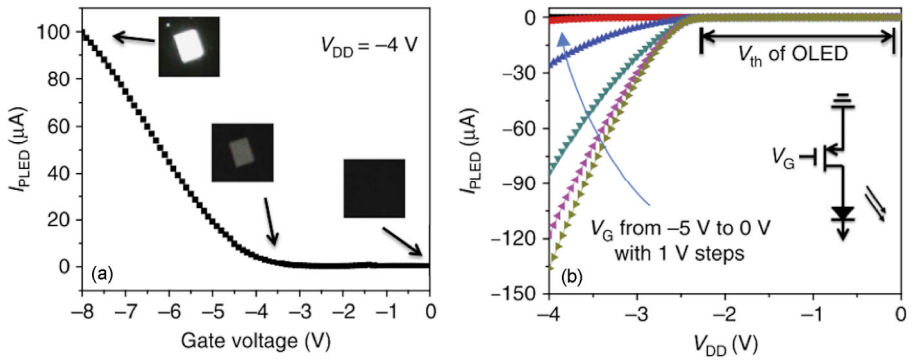

Figure 14 (a) I_{OLED} as a function of V_G with V_{DD}=–4.0 V. The OLEDs at different brightness are shown in the insets correlated to specific V_G values. (b) Output characterisitcs of the OLED control circuit as a function of gate voltage, with a schematic diagram of the OLED control circuit in the inset (color online). Reprinted with permission from ref. [37]. Copyright {2015} Nature Publishing Group.

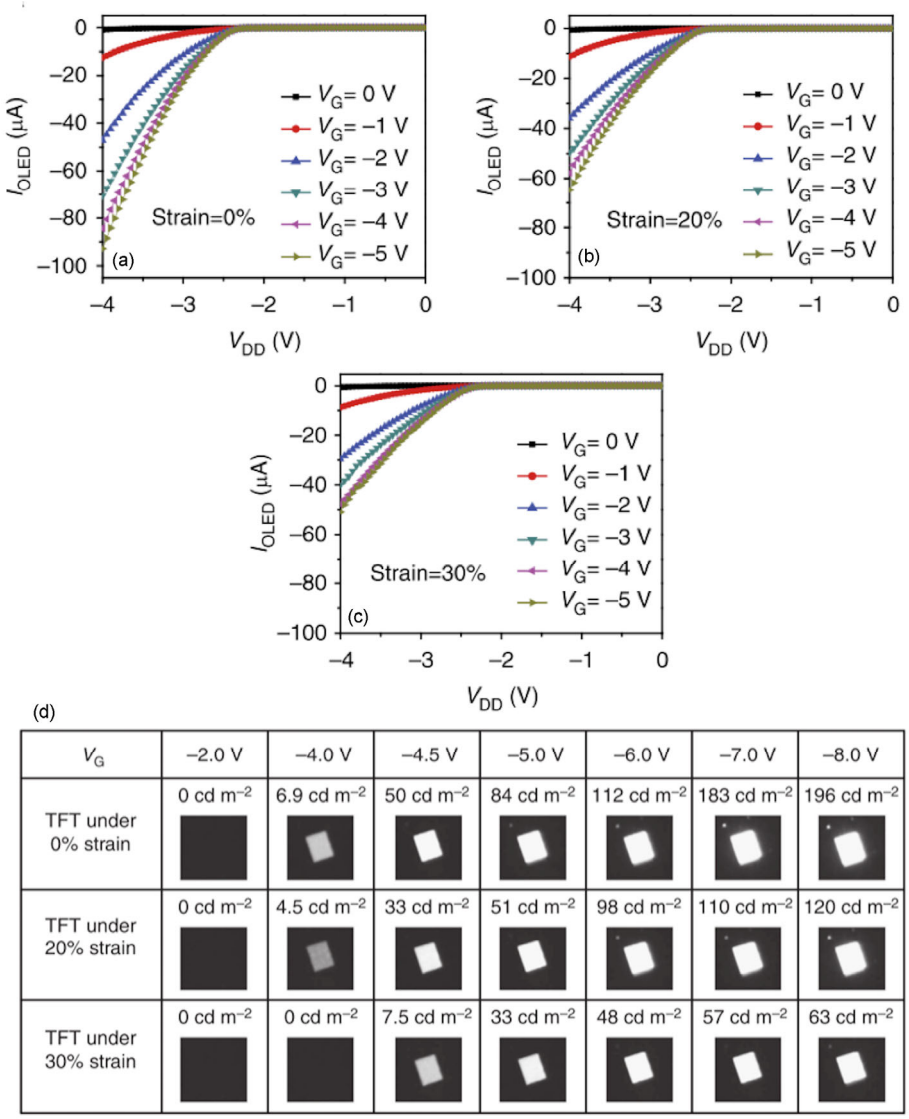

Figure 15 (a) Output characteristics of the OLED controlled by the stretchable TFT at 0% strain along the channel length direction. (b) Output characteristics of the OLED controlled by the stretchable TFT at 20% strain along the channel length direction. (c) Output characteristics of the OLED controlled by the stretchable TFT at 30% strain along the channel length direction. (d) Luminance of an OLED driven by stretchable TFTs under different inputs (color online). Reprinted with permission from ref. [37]. Copyright {2015} Nature Publishing Group.

als can be embedded within a polymer matrix to form conductive electrodes with low roughness for optoelectronic applications. The versatility of these electrodes allows for a wide range of devices to be fabricated on top, ranging from various lighting devices, TFT arrays, and capacitive sensors. Furthermore, the properties of the electrodes can be tailored individually for the application at hand.

Polymer light emitting electrochemical cells, polymer light emitting diodes, and transistors have been discussed at length in this review. Additional applications that have been demonstrated on the basis of the technology discussed include solar cells, touch sensors, and actuators. Further improvements on applications based on these alternative TCEs continue, rapidly driving demand for next generation devices. As for the basis of the TCE technology itself, the fabrication and processing of the electrodes in and of itself has reached a relatively mature stage. However, new process developments to further reduce financial consideration of this developing technology are still critical. These alternative TCEs already promise cheaper devices than respective devices built on traditional ITO technology. An analysis conducted by Emmott *et al*. [38] found that AgNW electrodes have the potential to reduce device cost per Watt by 17%. A rough estimation by this group found that for OLED substrates, the cost per meter is slightly lower for AgNW based electrodes when compared to ITO, though the AgNW based substrate is able to more than double the efficiency of the lighting device compared to ITO. However, these estimations do not take into account the potential for degradation and shorter lifetimes of devices built on these

substrates.

Thus, the most critical TCE improvement involves improving the stability of AgNW and SWCNT electrodes. These factors such as process reproducibility, yield, thermal stability, and operational stability in extreme usage conditions will serve to greatly expedite the future of wearable electronics. Continual improvements and development promise a myriad of stretchable and wearable electronics, bringing us one step closer to the futuristic vision of electronics envisioned for so many years.

Acknowledgments This work was supported in part by the Air Force Office of Scientific Research (FA9550-12-1-0074, Dr. Charles Lee).

Conflict of interest The authors declare that they have no conflict of interest.

1 Kumar A, Zhou C. *ACS Nano*, 2010, 4: 11–14
2 Rowell MW, Topinka MA, McGehee MD, Prall HJ, Dennler G, Sariciftci NS, Hu L, Gruner G. *Appl Phys Lett*, 2006, 88: 86–89
3 Zhang D, Ryu K, Liu X, Polikarpov E, Ly J, Tompson ME, Zhou C. *Nano Lett*, 2006, 6: 1880–1886
4 Kim KS, Zhao Y, Jang H, Lee SY, Kim J M, Kim KS, Ahn JH, Kim P, Choi JY, Hong BH. *Nature*, 2009, 457: 706–710
5 Bae S, Kim H, Lee Y, Xu X, Park JS, Zheng Y, Balakrishnan J, Lei T, Kim HR, Song YII, Kim YJ, Kim KS, Özyilmaz B, Ahn JH, Hong BH, lijima S. *Nat Nanotechnol*, 2010, 5: 574–578
6 Ellmer K. *Nat Photonics*, 2012, 6: 808–816
7 Zeng XY, Zhang QK, Yu RM, Lu CZ. *Adv Mater*, 2010, 22: 4484–4488
8 Langley D, Giusti G, Mayousse C, Celle C, Bellet D, Simonato JP. *Nanotechnology*, 2013, 24: 452001
9 Lee Y, Suh M, Kim D, Lee D, Chang H, Lee HS, Kim YW, Kim T, Suh KS, Jeon DY. *Adv Funct Mater*, 2014, 24: 6465–6472
10 Song M, Park JH, Kim CS, Kim DH, Kang YC, Jin SH, Jin WY, Kang JW. *Nano Res*, 2014, 7: 1370–1379
11 Jin J, Lee J, Jeong S, Yang S, Ko JH, Im HG, Baek SW, Lee JY, Bae BS. *Energy Environ Sci*, 2013, 6: 1811-1817
12 Zhang X, Yan X, Chen J, Zhao J. *Carbon*, 2014, 69: 437–443
13 Yu C, Wu H, Chien C. *Jpn J Appl Phys*, 2015, 54: 081101
14 Liu HC, Lai YC, Lai CC, Wu BS, Zan HW, Yu P, Chueh YL, Tsai CC. *ACS Appl Mater Interf*, 2015, 7: 232–240
15 Huang GW, Xiao HM, Fu SY. *Nanoscale*, 2014, 6: 8495–8502
16 Wu J, Agrawal M, Becerril A, Bao Z, Liu Z, Chen ŕY, Peumans P. *ACS Nano*, 2010, 4: 43–48
17 Yu Z, Hu L, Liu Z, Sun M, Wang M, Grüner G, Pei Q. *Appl Phys Lett*, 2009, 95: 2007–2010
18 Yu Z, Liu Z, Wang M, Sun M, Lei G, Pei Q. *J Photonics Energy*, 2011, 1: 011003
19 Yu Z, Li L, Zhang Q, Hu W, Pei Q. *Adv Mater*, 2011, 23: 4453–4457
20 Li L, Yu Z, Hu W, Chang CH, Chen Q, Pei Q. *Adv Mater*, 2011, 23: 5563–5567
21 Yu Z, Zhang Q, Li L, Chen Q, Niu X, Liu J, Pei Q. *Adv Mater*, 2011, 23: 664–668
22 Li J, Liang J, Jian X, Hu W, Li J, Pei Q. *Macromol Mater Eng*, 2014, 299: 1403–1409
23 Yuan W, Hu L, Yu Z, Lam T, Biggs J, Ha SM, Xi D, Chen B, Senesky MK, Grüner G, Pei Q. *Adv Mater*, 2008, 20: 621–625
24 Brochu P, Stoyanov H, Chang R, Niu X, Hu W, Pei Q. *Adv Energy Mater*, 2014, 4: 1–9
25 Hu L, Yuan W, Brochu P, Gruner G, Pei Q. *Appl Phys Lett*, 2009, 94: 5–8
26 Yu Z, Niu X, Liu Z, Pei Q. *Adv Mater*, 2011, 23: 3989–3994
27 Hu W, Niu X, Li L, Yun S, Yu Z, Pei Q. *Nanotechnology*, 2012, 23: 344002
28 Yun S, Niu X, Yu Z, Hu W, Brochu P, Pei Q. *Adv Mater*, 2012, 24: 1321–1327
29 Hu W, Niu X, Zhao R, Pei Q. *Appl Phys Lett*, 2013, 102: 083303
30 Liang J, Li L, Niu X, Yu Z, Pei Q. *Nat Photonics*, 2013, 7: 817–824
31 Liang J, Li L, Tong K, Ren Z, Hu W, Niu X, Chen Y, Pei Q. *ACS Nano*, 2014, 8: 1590–1600
32 Yu Z, Sun M, Pei Q. *J Phys Chem B*, 2009, 113: 8481–8486
33 Yu Z, Wang M, Lei G, Liu J, Li L, Pei Q. *J Phys Chem Lett*, 2011, 2: 367–372
34 Liang J, Li L, Niu X, Yu Z, Pei Q. *J Phys Chem C*, 2013, 117: 16632–16639
35 Li L, Yu Z, Chang C, Hu W, Niu X, Chen Q, Pei Q. *Phys Chem Chem Phys*, 2012, 14, 14249-14254
36 Li L, Liang J, Chou SY, Zhu X, Niu X, Yu Z, Pei Q. *Sci Rep*, 2014, 4: 4307
37 Liang J, Li L, Chen D, Hajagos T, Ren Z, Chou SY, Hu W, Pei Q. *Nat Commun*, 2015, 6: 7647
38 Emmott CJM, Urbina A, Nelson J. *Sol. Energy Mater Sol Cells*, 2012, 97: 14–21